MOF-Derived Co_3O_4 Nanoparticles Catalyzing Hydrothermal Deoxygenation of Fatty Acids for Alkane Production

Defu Zeng, Yalin Li, Tao Xia, Fuyi Cui, and Jing Zhang*

ACCESS | Metrics & More | Article Recommendations | SI Supporting Information

ABSTRACT: Designing economical and nonprecious catalysts with a catalytic performance as good as that of noble metals is of great importance in future renewable bioenergy production. In this study, the metal−organic framework (MOF) was applied as a precursor template to synthesize Co_3O_4 nanoparticles with a carbon matrix shell (denoted as M-Co_3O_4). To select the synthesized optimal catalyst, stearic acid was chosen as the model reactant. The effects of catalyst dosage, methanol dosage, water dosage, temperature, and reaction time on catalytic efficiency were examined. Under the designed condition, M-Co_3O_4 exhibited high catalytic performance and the catalyst showed higher conversion of stearic acid (98.7%) and selectivity toward C8−C18 alkanes (92.2%) in comparison with Pt/C (95.8% conversion and 93.2% selectivity toward C8−C18). Furthermore, a series of characterization techniques such as scanning electron microscopy (SEM), high-resolution transmission electron microscopy (HRTEM), X-ray powder diffraction (XRD), X-ray photoelectron spectroscopy (XPS), nitrogen adsorption isotherms (Brunauer−Emmett−Teller (BET) method), and thermogravimetric analysis (TGA) was applied to investigate the physicochemical properties of the catalysts. Finally, we proposed that decarbonization (deCO) could be the presumably mechanistic pathway for the production of C8−C18 alkanes from the decomposition of stearic acid.
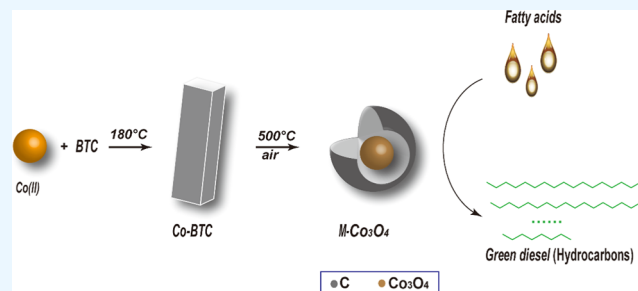
INTRODUCTION

Biomass energy is one of the most significant renewable energy sources.[1] Green diesel has drawn remarkable attention because it is easy to integrate with current refinery and transportation infrastructure as a substitute to prevalent fuel.[2] In addition, the green diesel achieves the necessities specified by the standard of European diesel fuel and can favorably resolve the pour and cloud point matters.[3] Hence, untapped abundant waste greases could generate a huge amount of clean energy, which would perform a critical role in alleviating the challenges of environmental pollution and greenhouse gas emissions. Different feedstocks (e.g., animal fats, vegetable oils, and waste oils) employed for the production of biodiesel are mainly composed of triacylglycerides (a triglyceride is an ester derived from three fatty acids and glycerol) and free fatty acids. Therefore, the key to the output of green diesel is the deoxygenation of fatty acids.[4] Especially, many metal catalysts, both noble and non-noble, have been studied; however, the optimization of the synthesis process and catalytic reaction conditions of the catalysts are still a work in progress.

Currently, the advancement of non-noble metal catalysts is becoming increasingly crucial due to the deficiency and high cost of noble metals. Several varieties of materials such as zeolites, bimetallic materials, composite transition metals, oxides, metal sulfide, and other acid catalysts[5−8] have been substantially studied in the catalytic conversion of esters/fatty acids. Among the non-noble catalysts, due to the vigorous

redox potentials of transition metals, they are the potentially important options for the production of green diesel from fatty acids. Metal−organic frameworks (MOFs) are functional materials with framework structures formed by metal atoms and organic ligands through coordination bonds, which possess various unique properties such as open metal sites, permanent porosity, high specific surface area, and chemical tenability.[9,10] They are ideal precursors for the preparation of composites composed of carbons and metal nanoparticles.[11] Under high-temperature conditions, regularly ordered metal centers in MOFs would be converted into metal nanoparticles in situ. In addition, attributable to the confinement impact of MOFs, a large number of ligands are thermally decomposed to build carbon matrix materials,[12,13] which can effectively restrain the aggregation of nanoparticles by immobilizing the highly distributed metal particles via charge-transfer and mechanical interactions.[13] To this end, metal nanoparticle composite materials with durable structure and good dispersibility of nanoparticles can be synthesized. For example, scholars have

synthesized MOF-derived composites with sandwich-type and core−shell structures and studied the catalytic properties of the materials.[14,15] However, to the best of our knowledge, such composites are rarely used to catalyze the deoxygenation of fatty acids to produce green diesel.

Fatty acids are frequently generated in the aqueous phase in many previous research studies on biofuel production.[16] When using triglycerides as a raw material for biodiesel production, hydrolysis of triglycerides to generate fatty acids is the first step. The ordinary method is to separate and gather fatty acids and transform them into biofuel. However, immediate hydrothermal deoxidization of fatty acids to produce hydrocarbons makes the process simpler because it does not require the separation and purification of fatty acids. On the other hand, Fu et al.[16] specified that H_2 can be produced in situ during the hydrothermal catalysis of fatty acids, which is advantageous for the process of hydrodeoxygenation (HDO).

In this work, the MOFs Co-BTC, Ni-BTC, and Cu-BTC were chosen as precursors to prepare the MOF-derived M-Co_3O_4, M-NiO, and M-CuO catalysts for the production of green diesel from fatty acids. This research aims to evaluate the activity of different MOF-derived materials (M-Co_3O_4, M-NiO, and M-CuO) and compared them with a precious catalyst (Pt/C) in an aqueous phase. The screening of optimal catalyst and reaction conditions was carried out with stearic acid as the model reactant of waste greases. The catalytic performance of M-Co_3O_4 in the deoxygenation and cleavage reactions during the transformation of stearic acid was examined. In brief, conclusions from this research indicate the promise of MOF-derived materials as cost-effective catalysts in the production of green diesel from waste greases.

■ EXPERIMENTAL METHODS

Preparation of MOF-Derived Catalysts. The synthesis process of MOFs is consistent with our previous study[17] and draws on the research by Chowdhury et al.[18] During the synthesis of cobalt, nickel, and copper MOFs, cobalt nitrate hexahydrate ($Co(NO_3)_2 \cdot 6H_2O$), nickel nitrate hexahydrate ($Ni(NO_3)_2 \cdot 6H_2O$), and copper nitrate trihydrate ($Cu(NO_3)_2 \cdot 3H_2O$) were utilized as an inorganic metal center and 1,3,5-benzenetricarboxylic acid (H_3BTC) as the organic linking ligands. Specifically, taking M-Co_3O_4 as an example, 0.42 g (2 mmol) of H_3BTC was dissolved in a 1:1 (v/v) mixed ethanol/ N,N-dimethylformamide (DMF) solvent in a volume of 40 mL and $Co(NO_3)_2 \cdot 3H_2O$ (2.095 g, 7.2 mmol) was dissolved in 15 mL of the aqueous phase. The two solutions were then mixed and stirred at room temperature for 30 min. Whereafter, the mixed solution was transferred to an autoclave and kept at a specific temperature and for a specific time (the synthesis temperature and time of Co-BTC and Ni-BTC were 180 °C and 12 h, and the synthesis temperature and time of Cu-BTC were 120 °C and 10 h, respectively). The reactor was then cooled to room temperature spontaneously. The contents of the reactor were then taken out to be centrifuged and then washed with ethanol and water several times. The acquired crystals were dried under a vacuum and kept for 5 h at 80 °C. The Co-MOF was obtained immediately. The MOF-derived material can be obtained by calcining the product at 500 °C for 2 h in an air atmosphere.

Characterization of Catalysts. The morphologies Co-MOF and M-Co_3O_4 were characterized by scanning electron microscopy (SEM, JEOL JSM-7800F, Kabushiki Kaisha), and the operating voltage of the X-ray tube was 15 kV. A high-resolution transmission electron microscope (HRTEM, Talos F200S, Thermofisher Scientific) operated at 200 kV was used to examine the micrographs of M-Co_3O_4. HRTEM, energy-dispersive X-ray spectroscopy (EDS), and high-angle annular dark field scanning transition electron microscopy (HAADF-STEM) measurements performed at 200 kV were combined to characterize the crystal structure and elemental distribution of M-Co_3O_4. X-ray diffraction (XRD, D8 Advance, Bruker) was used to study the constitution of the synthesized materials, and Cu $K\alpha$ (λ = 0.154) was utilized as a source of radiation. The specific surface area, pore volume, and pore size distribution of M-Co_3O_4 were determined by the Brunauer−Emmett−Teller (BET) method and the Barrett−Joyner−Halenda (BJH) method combined with nitrogen adsorption−desorption isotherms measured by Quadrasorb 2MP. The thermal transformation properties of Co-MOF were examined using a thermogravimetric analyzer (TGA, TGA/DSC 1/1600, Mettler Toledo). X-ray photoelectron spectroscopy (XPS, Escalab 250Xi, Thermofisher Scientific) measurements were used to investigate the surface valence states of the catalyst M-Co_3O_4 before and after the reaction.

Hydrothermal Procedure. All experiments in this study were performed in a 1.67 mL volume microreactor produced by Swagelok, which was assembled according to the reactor used by Fu et al.[19] and in our previous study.[17] Specifically, 15 mg of catalyst, 500 μL of water, 15 mg of methanol, and 0.176 mmol of stearic acid were charged into a microreactor and sealed. The tube furnace was first heated to the specified temperature, and then the reactor was placed in the tube furnace for a certain period of time. In particular, to ensure that the reactant concentration gradient and temperature gradient in the reactor did not affect the experimental results, the quartz tube in the furnace was rotated at 180° per 5 min. Such an operation has been shown to be feasible in our previous research.[17] After the reaction, the reactor was taken out and quickly put into water to stop the reaction. Subsequently, the compound in the reactor was flushed out with chloroform and made the solution to constant volume with chloroform and water in the volumetric flask, respectively. After suctioning off the water in the upper layer, the chloroform solution was analyzed by the liquid phase. The reused catalyst was obtained by centrifuging the remaining mixture in the volumetric flask after centrifuging.

Product Analysis. The concentration of solution products was examined using a gas chromatograph GC 7890B from Agilent with a flame ionization detector (FID) and an automatic sampler in this research. The samples were quantitatively analyzed using a gas chromatography-hydrogen flame ionization detector (GC-FID, Agilent 7890B). The column was an Agilent HP-5 capillary column (30 m × 0.32 mm × 0.25 μm). The injection temperature, injection volume, split ratio, and FID detection temperature were 280 °C, 1 μL, 10:1, and 300 °C, respectively. The programmed heating process was first kept at 60 °C for 1 min and then heated to 290 °C at a rate of 8 °C/min. In this study, the external standard method was used to quantitatively analyze the results of GC-FID, and the mixed C8−C20 alkane standards purchased by Sigma-Aldrich were used for the quantitative analysis of the liquid product.

The conversion, molar yield, and selectivity presented in this paper are derived from the following three equations.
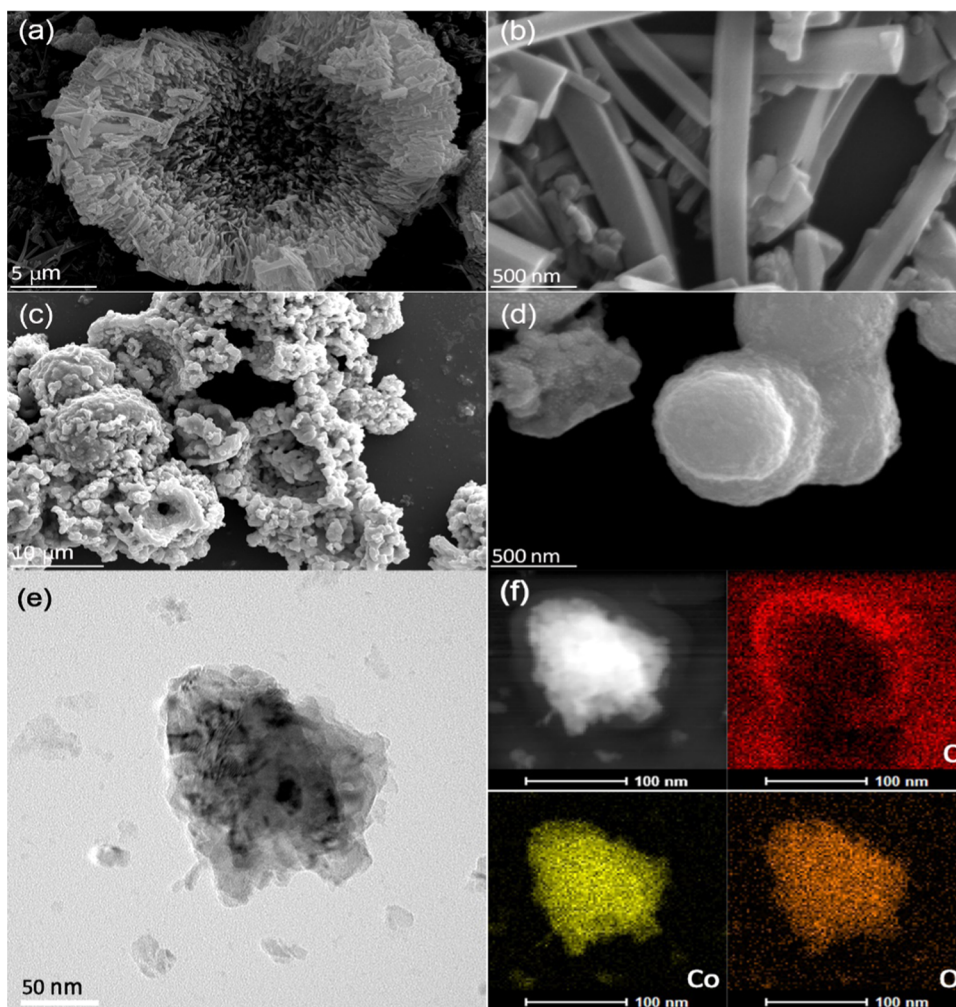
Figure 1. SEM of (a, b) Co-BTC and (c, d) M-Co$_3$O$_4$. (e) HRTEM image of M-Co$_3$O$_4$. (f) HAADF image of M-Co$_3$O$_4$ and the EDS spectra of C, Co, and O.

conversion (mol %)

$$= \left(1 - \frac{\text{moles of fatty acids after reaction}}{\text{moles of fatty acids introduced}}\right) \times 100\% \quad (1)$$

molar yield (mol %)

$$= \frac{\text{moles of each liquid product}}{\text{moles of fatty acids introduced}} \times 100\% \quad (2)$$

selectivity (mol %)

$$= \frac{\text{moles of each product}}{\text{moles of fatty acids introduced} - \text{moles of fatty acids after reaction}}$$
$$\times 100\% \quad (3)$$

■ RESULTS AND DISCUSSION

Catalyst Characterization. The crystal texture images of Co-BTC and M-Co$_3$O$_4$ are characterized by SEM, as presented in Figure 1a,b. Consistent with the previous research,[20] the Co-BTC is composed of rhabdoid-shaped microcrystals. As for M-Co$_3$O$_4$ (Figure 1c,d), totally different structure was observed, and the shape of M-Co$_3$O$_4$ nanospheres was assembled by nanoparticles. Therefore, it can be inferred that the organic components in MOFs are decomposed and liberated from the solid crystals during conversion.

HRTEM image of M-Co$_3$O$_4$ clearly shows a core—shell structure (Figure 1e). As shown in Figure 1f, the distribution of the elements in the catalyst crystals was detected by HAADF and EDS. This characterization method successfully revealed the elemental distribution of C, O, and Co, which indicated that Co-BTC was transformed into a composite material with a "metal-oxide/carbon" structure, which suggested that BTC ligands were converted to carbon during calcination.[15] In addition, it can be seen from the element distribution that the X-ray signal distribution of Co and O is extremely uniform, which indicated that the oxidation state of cobalt is anchored on the carbon shell. Since the ligand-derived carbon shell can immobilize the Co$_3$O$_4$ nanoparticles, which could restrain the evolution of nanoaggregates,[21] this feature is beneficial to the activity of the catalyst.

As shown in Figure S1a, the diffraction peaks appear at 15.2, 17.7, 18.9, 27.1, 32.8, 34.0, and 35.7° for Co-BTC can be ascribed to [Co$_3$(BTC)$_2$(H$_2$O)$_{12}$],[20,22,23] which indicates that MOF precursors Co-BTC are assuredly synthesized. As depicted in Figure S1b, obvious diffraction peaks of C, Co, and Co$_3$O$_4$ appear in the XRD patterns. Specifically, combined with the characterization results in Figure 1f, it is speculated that the broad diffraction peak (between 15 and 30°) reflects

the carbon shell formed by the transformation of BTC at high temperature. The peaks at 36.8 and 59.4° can be indexed to Co_3O_4. In contrast with X-ray maps of C, Co, and O (Figure 1f), significant Co^0 peaks located at 44.2, 51.5, and 75.9° indicate that the Co core is encapsulated by Co_3O_4.

Figure S2 presents the TGA image of the Co-BTC precursor. Between 0 and 265 °C in the first stage, the mass of the sample slowly decreased by 12.7% due to the evaporation of N,N-dimethylformamide (DMF) and water molecules from the precursor material.[24] As the temperature continued to increase, a rapid mass loss was observed due to the decomposition of BTC ligands and MOF framework.[24] Combined with the characterization of electron microscopy and XRD, it can be speculated that the Co ions were converted into Co and Co_3O_4 in the heating procedure. The percent mass loss determined by TGA was close to the theoretical results (39.9% theoretical residue compared with 35.4% residue determined by TGA), which indicated the existence of ~11% impurities in Co-BTC. When the temperature was increased to over 500 °C, no further mass loss was discovered, which suggested that the Co-MOF precursor had been completely converted into $M-Co_3O_4$ nanoparticles, which were durable under high temperature. Thus, 500 °C was chosen as the temperature to synthesize the $M-Co_3O_4$ catalyst in this research.

The N_2 adsorption−desorption isotherm of $M-Co_3O_4$ and the pore size distribution of the catalyst are shown in Figure S3, and Table 1 depicts the texture properties of the three

Table 1. Texture Properties of $M-Co_3O_4$, M-NiO, and M-CuO

catalyst	BET surface area (m^2/g)	pore volume (cm^3/g)	average pore diameter (nm)	reference
M-CuO	5.1	0.007	3.3	17
M-NiO	16.3	0.071	3.3	17
$M-Co_3O_4$	6.8	0.008	3.3	this study

catalysts. In our previous study,[17] M-CuO can be classified into an H2 hysteresis loop (type IV isotherm), which indicates that the presence of ink-bottle pores in M-CuO was usual in inorganic oxides. M-NiO and $M-Co_3O_4$ can be assigned to H3 hysteresis loops (type IV isotherms), indicating the existence of hierarchical mesoporous structures in the materials. The N_2 adsorption−desorption isotherms of $M-Co_3O_4$ and M-CuO showed smaller hysteresis loops compared with M-NiO, which resulted in scarce surface areas (6.8 m^2/g for $M-Co_3O_4$ and 5.1 m^2/g for M-CuO). M-NiO possessed a larger hysteresis loop, and its BET surface area was much higher (16.35 m^2/g). Particularly, because pores are created by the decomposition of the ligands and framework, the pore size distributions of all three catalysts indicate that pores are around 3−5 nm, which is much smaller than those in ordinary metal oxides.[17]

XPS measurement was used to affirm the metal oxidation states and the chemical compositions of the synthesized material. The C 1s spectrum of the catalyst is shown in Figure 2a, and the sample displayed several different functional groups. The functional group appearing at 284.8 eV was nonoxidized C=C/C−C, at 286.3 eV was C−O/C−O−C, and at 288.7 eV was the carbon in C=O/O−C=O.[25] The Co 2p spectrum (Figure 2b) shows a $2p_{1/2}$ peak at 795.9 eV, as well as a $2p_{3/2}$ peak at 780.2 eV, affirming the existence of Co^{II}. In addition, the $2p_{1/2}$ and the $2p_{3/2}$ peaks at 793.8 and 778.7

eV, respectively, were attributed to Co^{III}.[26,27] Consistent with the research of Xia et al.,[28] no significant Co^0 peak is found in Figure 2b, indicating that the surface layer of $M-Co_3O_4$ is easily oxidized, and the oxidized Co_3O_4 shell can well prevent the oxidation of the Co core. The XPS spectrum of O 1s in $M-Co_3O_4$ is shown in Figure 2c. The O 1s spectrum was deconvolved into the main peak with two shoulder peaks. Specifically, the peaks at 529.5 and 532.1 eV corresponded to the lattice oxygen and the so-called "metal−oxygen" bond ($O_{lattice}$, Co−O), while the peak located at 531.0 eV was assigned to the adsorbed oxygen ($O_{adsorbed}$).[17]

The chemical valence and the species of oxygen in the used $M-Co_3O_4$ were investigated by XPS (Figure 2d−f). As shown in Figure 2d, the spectrum of C 1s barely changed, which indicated that the carbon matrix remained stable during the reaction and can still act as a support and stabilize the highly dispersed metal nanoparticles through the charge transfer and mechanical interactions and restrain the aggregation. Oxygen vacancies are one of the most common defects in metal oxides. It has been reported[29] that the redox performance of catalysts is related to the number of oxygen vacancies in oxide catalysts. As illustrated in Figure 2, a significant amount of Co^0 was produced in $M-Co_3O_4$ during the reaction (Figure S2b vs Figure 4e), and the content of adsorbed oxygen on the surface of $M-Co_3O_4$ increased significantly due to the conversion of $Co^{III}/Co^{II}/Co^0$ (Figure S2c vs Figure 4f), which indicated that $M-Co_3O_4$ generated a large number of oxygen vacancies during the deoxygenation process,[30] which was in favor of the improvement in catalytic performance.

Catalyst Screening. The catalytic activities of Pt/C and synthesized monometallic catalysts M-CuO, M-NiO, and $M-Co_3O_4$ were comparatively studied with those of stearic acid as a model reactant. As shown in Figure 3, the conversion of stearic acid catalyzed by Pt/C and synthesized M-CuO, M-NiO, and $M-Co_3O_4$ depicted obvious differences of 95.8% for Pt/C, 55.8% for M-CuO, 70.9% for M-NiO, and 98.7% for $M-Co_3O_4$. The selectivity of several catalysts for the transformation of stearic acid to C8−C18 also varied considerably. When M-CuO and M-NiO were used as catalysts, a large amount of octadecanol was detected in the products, especially 23.7% for M-CuO and 20.7% for M-NiO. Nevertheless, a small quantity of octadecanol (<1%) was detected when $M-Co_3O_4$ was used as a catalyst. Especially, the selectivity toward all C8−C18 and heptadecane in the products when $M-Co_3O_4$ was used as a catalyst reached 92.2 and 59.7%, respectively, which far exceeded the selectivity in the corresponding products when M-CuO and M-NiO were used as catalysts. Therefore, among the three synthesized catalysts, $M-Co_3O_4$ had the best activity in catalyzing the deoxygenation of stearic acid. Notably, $M-Co_3O_4$ easily catalyzed the cleavage of the C−C bonds in comparison with Pt/C (the selectivity toward alkanes of C8−C16 was 28.2% over $M-Co_3O_4$, while 17.8% over Pt/C). In conclusion, $M-Co_3O_4$ possessed the best catalytic performance for stearic acid among the three synthesized catalysts. Hence, $M-Co_3O_4$ was selected for further study of the influencing factors and mechanism.

Optimization of Reaction Conditions. As depicted in Figure 4a, as the reaction time increased to 80 min, the conversion of stearic acid reached 98.7%. At the beginning of the process, the main product was octadecanol, whose selectivity was 41.5% at 10 min. However, when the time reached 30 min, the selectivity towards octadecanol declined to 12.0%. When the time exceeded 80 min, the selectivity toward
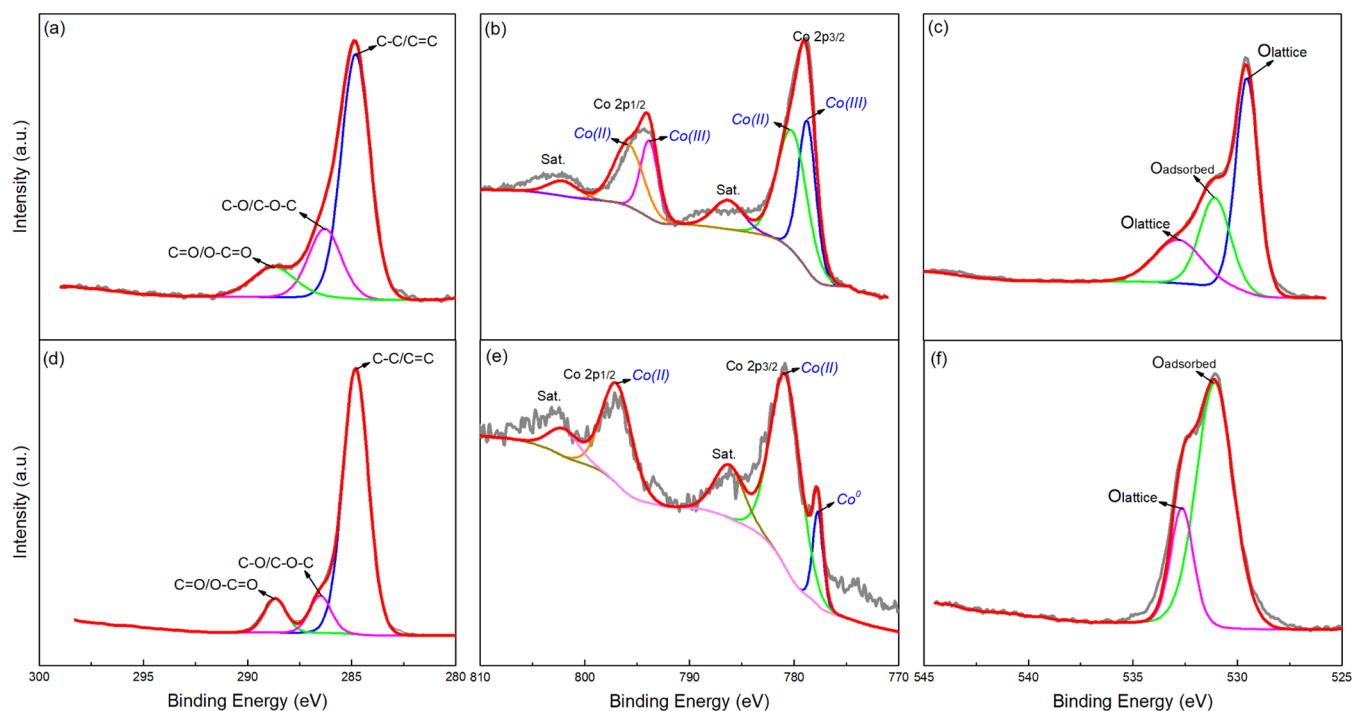
Figure 2. XPS spectra of fresh M-Co$_3$O$_4$ ((a) C 1s, (b) Co 2p, and (c) O 1s) and used M-Co$_3$O$_4$ ((d) C 1s, (e) Co 2p, and (f) O 1s).
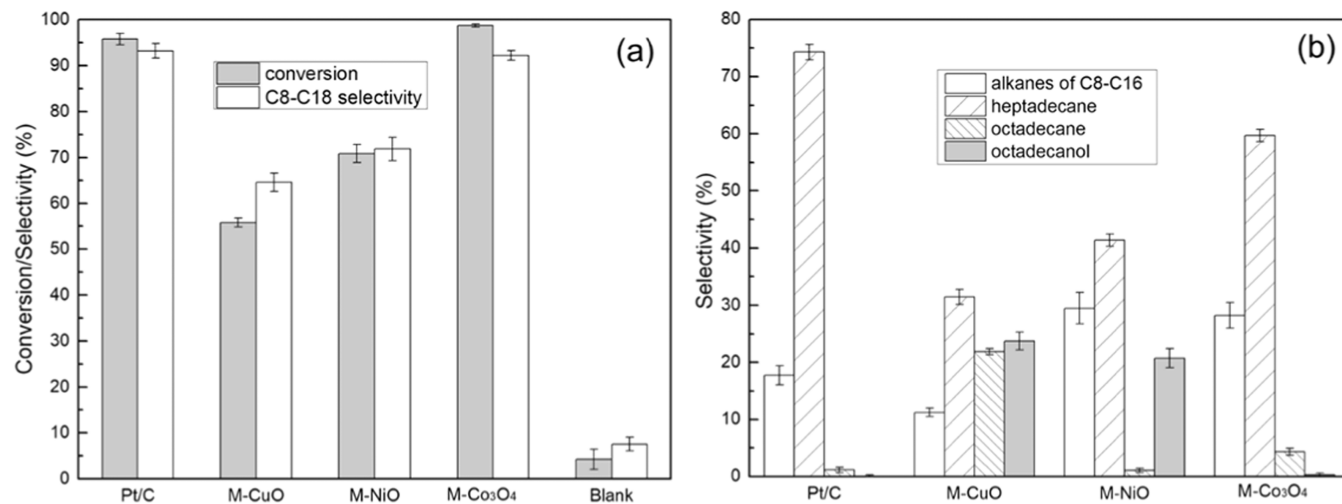

Figure 3. (a) Catalytic performance (the conversion of stearic acid and the selectivity of C8−C18) over different catalysts Pt/C, M-CuO, M-NiO, and M-Co$_3$O$_4$ for the transformation of stearic acid. (b) Deoxidized product distribution over Pt/C, M-CuO, M-NiO, and M-Co$_3$O$_4$. Reaction conditions: M-Co$_3$O$_4$ = 15 mg, stearic acid = 0.176 mmol, H$_2$O = 500 μL, methanol = 15 mg, T = 330 °C, and reaction time = 80 min.

octadecanol dropped to <1%. The phenomenon indicated that the major intermediate in the convertible reaction of stearic acid was octadecanol. The selectivity to heptadecane reached 67.7% at 30 min. As the reaction time progressed, a decreased selectivity toward heptadecane was observed. However, the selectivity toward C8−C16 was increased, indicating the cleavage of C−C bonds in heptadecane over a longer reaction time.

As shown in Figure 4b, with the temperature ranging from 280 to 330 °C, the conversion of stearic acid gradually increased and reached 98.7% at 330 °C. As the temperature continued to increase, the conversion exceeded 99% at 360 °C, which indicated that stearic acid was completely converted. The selectivity to heptadecane dropped from 71.0% at 280 °C to 30.4% at 360 °C, which suggested that the increased

temperature promoted the cleavage of C−C bonds to generate short-chain alkanes.[31]

The amount of hydrogen produced can be controlled by controlling the dosage of methanol since it extensively served as a hydrogen donor,[32] thereby affecting the transformation of greases. This research examined the effect of methanol dosage on the deoxygenation efficiency of stearic acid.[33] As depicted in Figure 4c, stearic acid can still undergo deoxygenation without the addition of methanol. On the one hand, the deoxygenation of stearic acid could occur through decarboxylation without the participation of hydrogen. On the other hand, Fu et al.[16] demonstrated that H$_2$ was generated in situ during the hydrothermal catalysis of fatty acids, which also enhanced the conversion of stearic acid. As methanol was added to the reaction and the dosage increased, the conversion
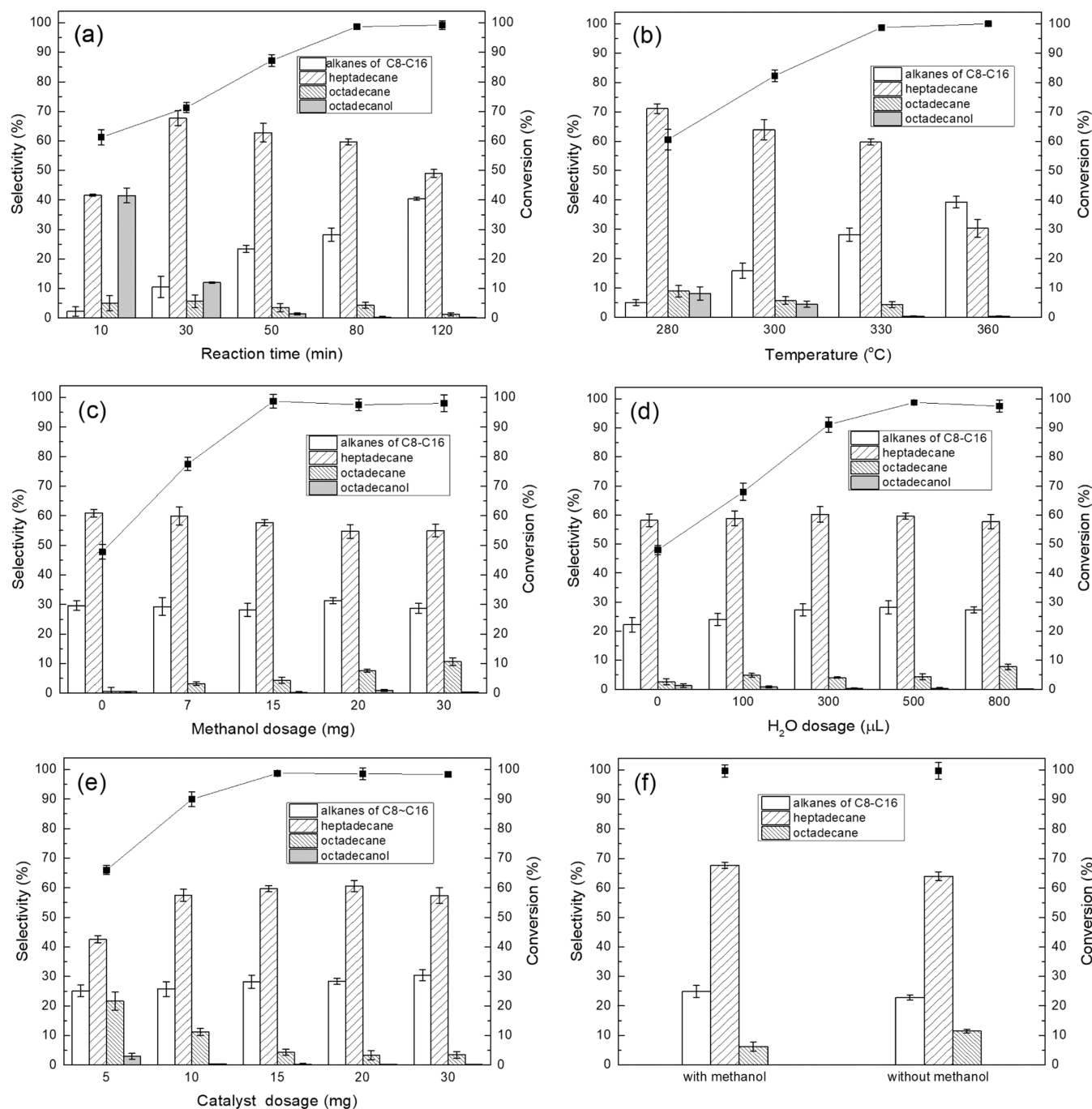
Figure 4. Catalytic performance of M-Co_3O_4 in changed reaction conditions and the role of methanol. (a) Reaction time. Reaction conditions: M-Co_3O_4 = 15 mg, stearic acid = 0.176 mmol, H_2O = 500 μL, methanol = 15 mg, and T = 330 °C. (b) Temperature. Reaction conditions: M-Co_3O_4 = 15 mg, stearic acid = 0.176 mmol, H_2O = 500 μL, methanol = 15 mg, and reaction time = 80 min. (c) Methanol dosage. Reaction conditions: M-Co_3O_4 = 15 mg, stearic acid = 0.176 mmol, H_2O = 500 μL, T = 330 °C, and reaction time = 80 min. (d) H_2O dosage. Reaction conditions: M-Co_3O_4 = 15 mg, stearic acid = 0.176 mmol, methanol = 15 mg, T = 330 °C, and reaction time = 80 min. (e) Catalyst loading. Reaction conditions: stearic acid = 0.176 mmol, H_2O = 500 μL, methanol = 15 mg, T = 330 °C, and reaction time = 80 min. (f) Product distribution of octadecanol catalyzed by M-Co_3O_4 with or without added methanol. Reaction conditions: M-Co_3O_4 = 15 mg, stearic acid = 0.176 mmol, H_2O = 500 μL, methanol = 15 mg (if added), T = 330 °C, and reaction time = 80 min.

of stearic acid increased rapidly and attained a maximum value (98.7%) at 15 mg. Nevertheless, while the dosage of added methanol was increased to 30 mg, the conversion remained almost unchanged. Cao et al.[34] stated that the Co^0 active centers encouraged the HDO routine of fatty acids. In this research, Co^{II} and Co^{III} in M-Co_3O_4 could be reduced to Co^0 by hydrogen produced from the decomposition of methanol.

Therefore, Co^0 generated by the reduction of Co^{II} and Co^{III} significantly enhanced the reaction rate of HDO and the overall reaction. As the dosage of methanol increased, the selectivity to heptadecane dropped moderately (from 60.9 to 55.0% when the dosage of methanol increased from 0 to 30 mg), while the selectivity to octadecane increased significantly (from 0.6 to 10.6% when the dosage of methanol increased
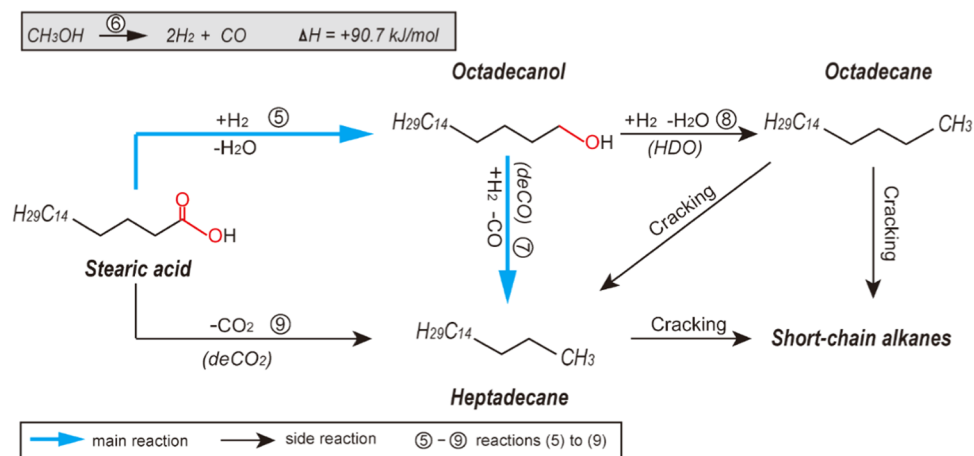
Figure 5. Reaction routines of stearic acid to C8–C18 alkanes over the M-Co$_3$O$_4$ catalyst.

from 0 to 30 mg). Since octadecane was produced through HDO from stearic acid, it is speculated that the increase in methanol could produce more hydrogen, which shifted the direction of the reaction toward the formation of octadecane.

The conversion of stearic acid increased steadily when the dosage of H$_2$O was raised from 0 to 500 μL and attained a maximum value (98.7%) at 500 μL (Figure 4c). While the dosage of H$_2$O was further added to 800 μL, the conversion remained unchanged. Furthermore, the selectivity toward alkanes of C8–C16 increased marginally (22.2% at 500 μL to 27.3% at 800 μL). In general, adding H$_2$O has only a minor influence on the selectivity of the products.

While the dosage of the M-Co$_3$O$_4$ catalyst was between 5 and 15 mg, there was a positive correlation between both the conversion of stearic acid and the selectivity toward alkanes of C8–C17 and the dosage of the catalyst (Figure 4e), which was consistent with the expectations since a larger amount of catalyst led to more active sites.[35] When the dosage of M-Co$_3$O$_4$ was further increased to 30 mg, the conversion remained nearly unchanged, which indicated that there were no side reactions caused by excessive active sites in this research. In addition, with the increase in catalyst dosage, the selectivity toward both octadecanol and octadecane dropped (as the dosage of M-Co$_3$O$_4$ increased from 5 to 30 mg, the selectivity toward octadecanol dropped from 2.9 to 0.2% and that toward the octadecane from 21.6 to 3.5%). Octadecane was the product of hydrodeoxygenation, suggesting that the decarbonization (deCO) of octadecanol to form heptadecane catalyzed by M-Co$_3$O$_4$ possessed a greater reaction rate compared with hydrodeoxygenation. The phenomenon was crucial since the deoxygenation of 1 mol stearic acid through decarbonization consumed 66.6% less hydrogen (Reaction Routines of Stearic Acid) than hydrodeoxygenation, suggesting that M-Co$_3$O$_4$ was an economical catalyst for the deoxygenation of fatty acid.
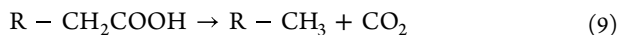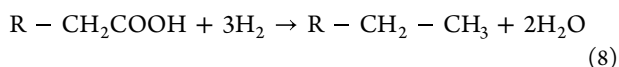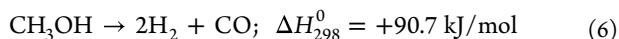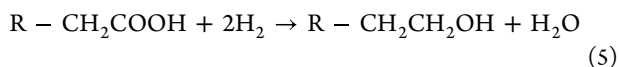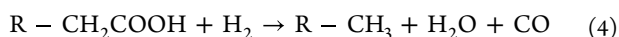
In summary, the reaction conditions of 15 mg of M-Co$_3$O$_4$, 500 μL of H$_2$O, 15 mg of methanol, temperature of 330 °C, and reaction time of 80 min were considered optimal conditions.

To further determine whether the production of heptadecane from octadecanol required the participation of hydrogen, octadecanol was used as a raw material under the same reaction conditions (15 mg of M-Co$_3$O$_4$, 15 mg of methanol, 500 μL of H$_2$O, temperature of 330 °C, and reaction time of 80 min) over M-Co$_3$O$_4$ with or without the added methanol.

As shown in Figure 4f, the deoxygenation of octadecanol and the selectivity toward different products were semblable, which affirmed that the transformation of octadecanol to heptadecane catalyzed by M-Co$_3$O$_4$ was a decarbonization process that did not need the participation of hydrogen.

The reusability of M-Co$_3$O$_4$ was examined under the optimal conditions (15 mg of M-Co$_3$O$_4$, 0.176 mmol stearic acid, 500 μL of H$_2$O, 15 mg of methanol dosage, temperature of 330 °C, and reaction time of 80 min). Figure S4 shows that the activity of the catalyst decreased slightly after use. Specifically, the conversion of stearic acid decreased from 98.7 to 85.0%. The phenomenon might be due to the fact that the active metal sites tend to dissolve in aqueous solutions, and the leaching of Co ions has a significant effect on the activity of the catalyst.[36] In addition, unavoidable carbon deposition on the surface of the catalyst might also be an important reason for the decreased activity.[37]

Reaction Routines of Stearic Acid. According to the aforementioned experiments and other literatures,[38,39] we put forward a feasible pathway for the production of green diesel from stearic acid over M-Co$_3$O$_4$ (reaction 4). As depicted in Figure 5, on the basis of Figure 4a,b, the first step of this reaction is the production of octadecanol from the hydrogenation of stearic acid (reaction 5), which demands the participation of hydrogen produced from the breakdown of methanol (reaction 6). Subsequently, the main product heptadecane is produced through a deCO pathway from the intermediate octadecanol (reaction 7). The excessive methanol could lead to more generation of octadecane through HDO (reaction 8). Furthermore, the deoxygenation of stearic acid can still occur without the participation of methanol since H$_2$ would be formed in situ during the hydrothermal catalytic process. In addition, alkanes of C8–C16 are generated from the cleavage of long-chain alkanes (heptadecane and octadecane). Toward this end, the desired products can be produced via the rationally designed reaction conditions, and the reaction rate could be compromised by minimizing external hydrogen inputs. For instance, in this study, by rationally controlling the dosage of methanol, the HDO pathway can be suppressed, and the deCO pathway can be enhanced. Additionally, the side reactions and energy consumption can be restrained by reasonably controlling the reaction temperature and time. Hence, the reaction can be carried out in the direction most conducive to the formation of the target products.

$$R - CH_2COOH + H_2 \rightarrow R - CH_3 + H_2O + CO \quad (4)$$

$$R - CH_2COOH + 2H_2 \rightarrow R - CH_2CH_2OH + H_2O \quad (5)$$

$$CH_3OH \rightarrow 2H_2 + CO; \quad \Delta H_{298}^0 = +90.7 \text{ kJ/mol} \quad (6)$$

$$R - CH_2CH_2OH \rightarrow R - CH_3 + CO + H_2 \quad (7)$$

$$R - CH_2COOH + 3H_2 \rightarrow R - CH_2 - CH_3 + 2H_2O \quad (8)$$

$$R - CH_2COOH \rightarrow R - CH_3 + CO_2 \quad (9)$$

Application of M-Co₃O₄ toward Other Fatty Acids.
The composition of waste greases in actual production is complex and contains various fatty acids. Therefore, the catalytic performance of distinct fatty acids (oleic, palmitic, and lauric acid) catalyzed by M-Co₃O₄ was compared, and the results are presented in Table 2. Almost complete decom-

Table 2. Catalytic Performance of the M-Co₃O₄ Catalyst towards Other Fatty Acids[a]

fatty acids	conversion (%)	selectivity towards alkanes of C8−C18 (%)
stearic acid	98.7	92.2
oleic acid	89.6	72.5
palmitic acid	>99	93.5
lauric acid	>99	91.8

[a]Reaction conditions: M-Co₃O₄ = 15 mg, stearic acid = 0.176 mmol, H_2O = 500 μL, methanol = 15 mg, T = 330 °C, and reaction time = 80 min.

position of the whole saturated fatty acids (>98%) and high selectivity toward alkanes of C8−C18 (>90%) were attained. However, oleic acid has not been completely deoxygenated, indicating that it is more difficult for M-Co₃O₄ to catalyze the deoxygenation of unsaturated fatty acids. As for saturated fatty acids, the length of the alkanes had no obvious influence on the selectivity toward alkanes of C8−C18, which was in agreement with the earlier study.[40]

CONCLUSIONS

M-Co₃O₄ is prepared using Co-BTC as a precursor for pyrolysis in air, which exhibits a comparable activity to Pt/C for the deoxygenation of stearic acid. Results from characterization and experiments indicated that the preferable catalytic performance of M-Co₃O₄ is partially ascribed to the textural properties (e.g., core−shell structure and pore size). Particularly, XPS of the utilized M-Co₃O₄ depicted that Co^{II} and Co^{III} in the catalyst were partially reduced to Co^0 during the reaction. The deoxygenation reaction was then promoted since the reduction of Co^{II} and Co^{III} significantly boosted the number of oxygen vacancies. As experimental conditions (time, temperature, and dosage of catalyst, methanol, water) were varied, it has been proved that the deoxygenation of stearic acid over M-Co₃O₄ mainly through hydrogenation and decarbonization pathways, which could greatly avail the saving of hydrogen compared with direct HDO. Furthermore, the production of green diesel from distinct fatty acids (oleic, palmitic, and lauric acid) catalyzed by M-Co₃O₄ was examined, and notable activities toward all fatty acids were observed consistently.

ASSOCIATED CONTENT

Supporting Information

The Supporting Information is available free of charge at https://pubs.acs.org/doi/10.1021/acsomega.2c04382.

XRD patterns, TGA curve, N₂ adsorption−desorption isotherm, and pore size distribution of catalyst; catalytic performance of fresh and used catalyst (PDF)

AUTHOR INFORMATION

Corresponding Author

Jing Zhang − School of Environment, Harbin Institute of Technology, Harbin 150090, P. R. China; College of Environment and Ecology, Chongqing University, Chongqing 400045, P. R. China; orcid.org/0000-0002-7518-3388; Email: zhangjing2018@cqu.edu.cn

Authors

Defu Zeng − School of Environment, Harbin Institute of Technology, Harbin 150090, P. R. China; College of Environment and Ecology, Chongqing University, Chongqing 400045, P. R. China

Yalin Li − Institute of Sustainability, Energy, and Environment, University of Illinois at Urbana−Champaign, Urbana, Illinois 61801, United States; orcid.org/0000-0002-8863-4758

Tao Xia − College of Environment and Ecology, Chongqing University, Chongqing 400045, P. R. China

Fuyi Cui − College of Environment and Ecology, Chongqing University, Chongqing 400045, P. R. China

Complete contact information is available at:
https://pubs.acs.org/10.1021/acsomega.2c04382

Notes

The authors declare no competing financial interest.

REFERENCES

(1) Adam Brown, P. F. Plotting a Path For Greater Bioenergy Use. https://www.iea.org/commentaries/plotting-a-path-for-greater-bioenergy-use (accessed June, 2017).

(2) Zhang, J.; Huo, X.; Li, Y.; Strathmann, T. J. Catalytic Hydrothermal Decarboxylation and Cracking of Fatty Acids and Lipids over Ru/C. ACS Sustainable Chem. Eng. 2019, 7, 14400−14410.

(3) Renewable Hydrocarbon Biofuels. https://afdc.energy.gov/fuels/emerging_hydrocarbon.html (accessed May 20, 2021).

(4) Liu, Y. Y.; Sotelo-Boyas, R.; Murata, K.; Minowa, T.; Sakanishi, K. Hydrotreatment of Vegetable Oils to Produce Bio-Hydrogenated Diesel and Liquefied Petroleum Gas Fuel over Catalysts Containing Sulfided Ni-Mo and Solid Acids. Energy Fuels 2011, 25, 4675−4685.

(5) Scaldaferri, C. A.; Pasa, V. M. D. Hydrogen-free process to convert lipids into bio-jet fuel and green diesel over niobium phosphate catalyst in one-step. Chem. Eng. J. 2019, 370, 98−109.

(6) Sudarsanam, P.; Zhong, R.; Van den Bosch, S.; Coman, S. M.; Parvulescu, V. I.; Sels, B. F. Functionalised heterogeneous catalysts for sustainable biomass valorisation. Chem. Soc. Rev. 2018, 47, 8349−8402.

(7) Yao, X.; Strathmann, T. J.; Li, Y.; Cronmiller, L. E.; Ma, H.; Zhang, J. Catalytic hydrothermal deoxygenation of lipids and fatty

acids to diesel-like hydrocarbons: a review. *Green Chem.* **2021**, *23*, 1114–1129.

(8) Liang, J.; Zhang, Z.; Wu, K.; Shi, Y.; Pu, W.; Yang, M.; Wu, Y. Improved conversion of stearic acid to diesel-like hydrocarbons by carbon nanotubes-supported CuCo catalysts. *Fuel Process. Technol.* **2019**, *188*, 153–163.

(9) Zhu, L.; Liu, X.-Q.; Jiang, H.-L.; Sun, L.-B. Metal-Organic Frameworks for Heterogeneous Basic Catalysis. *Chem. Rev.* **2017**, *117*, 8129–8176.

(10) Dhakshinamoorthy, A.; Li, Z.; Garcia, H. Catalysis and photocatalysis by metal organic frameworks. *Chem. Soc. Rev.* **2018**, *47*, 8134–8172.

(11) Wang, C.; Kim, J.; Tang, J.; Kim, M.; Lim, H.; Malgras, V.; You, J.; Xu, Q.; Li, J.; Yamauchi, Y. New Strategies for Novel MOF-Derived Carbon Materials Based on Nanoarchitectures. *Chem* **2019**, 19.

(12) Wang, Y.; Sang, S.; Zhu, W.; Gao, L.; Xiao, G. CuNi@C catalysts with high activity derived from metal−organic frameworks precursor for conversion of furfural to cyclopentanone. *Chem. Eng. J.* **2016**, *299*, 104–111.

(13) Dang, S.; Zhu, Q.-L.; Xu, Q. Nanomaterials derived from metal−organic frameworks. *Nat. Rev. Mater.* **2018**, *3*, No. 17075.

(14) Xu, J.; Xu, C.; Zhao, Y.; Wu, J.; Hu, J. Hollow Co$_3$O$_4$@MnO$_2$ Cubic Derived From ZIF-67@Mn-ZIF as Electrode Materials for Supercapacitors. *Front. Chem.* **2019**, *7*, No. 831.

(15) Guo, W. X.; Sun, W. W.; Wang, Y. Multilayer CuO@NiO Hollow Spheres: Microwave-Assisted Metal Organic-Framework Derivation and Highly Reversible Structure-Matched Stepwise Lithium Storage. *ACS Nano* **2015**, *9*, 11462–11471.

(16) Fu, J.; Lu, X.; Savage, P. E. Hydrothermal decarboxylation and hydrogenation of fatty acids over Pt/C. *ChemSusChem* **2011**, *4*, 481–486.

(17) Zeng, D. F.; Li, Y. L.; Ma, H. L.; Cui, F. Y.; Zhang, J. CuO@NiO Nanoparticles Derived from Metal-Organic Framework Precursors for the Deoxygenation of Fatty Acids. *ACS Sustainable Chem. Eng.* **2021**, *9*, 15612–15622.

(18) Chowdhury, P.; Bikkina, C.; Meister, D.; Dreisbach, F.; Gumma, S. Comparison of adsorption isotherms on Cu-BTC metal organic frameworks synthesized from different routes. *Microporous Mesoporous Mater.* **2009**, *117*, 406–413.

(19) Zhang, Z.; Yang, Q.; Chen, H.; Chen, K.; Lu, X.; Ouyang, P.; Fu, J.; Chen, J. G. In situ hydrogenation and decarboxylation of oleic acid into heptadecane over a Cu−Ni alloy catalyst using methanol as a hydrogen carrier. *Green Chem.* **2018**, *20*, 197–205.

(20) Shamaei, S.; Abbasi, A. R.; Noori, N.; Rafiee, E.; Azadbakht, A. Ultrasound-assisted coating of silk yarn with nano-porous Co$_3$(BTC)$_2$·12H$_2$O with iodine adsorption affinity. *Colloids Surf., A* **2013**, *431*, 66–72.

(21) Archana, V.; Xia, Y.; Fang, R.; Gnana kumar, G. Hierarchical CuO/NiO-Carbon Nanocomposite Derived from Metal Organic Framework on Cello Tape for the Flexible and High Performance Nonenzymatic Electrochemical Glucose Sensors. *ACS Sustainable Chem. Eng.* **2019**, *7*, 6707–6719.

(22) Dhakshinamoorthy, A.; Montero Lanzuela, E.; Navalon, S.; Garcia, H. Cobalt-Based Metal Organic Frameworks as Solids Catalysts for Oxidation Reactions. *Catalysts* **2021**, *11*, No. 95.

(23) Linnemann, J.; Taudien, L.; Klose, M.; Giebeler, L. Electro-deposited films to MOF-derived electrochemical energy storage electrodes: a concept of simplified additive-free electrode processing for self-standing, ready-to-use materials. *J. Mater. Chem. A* **2017**, *5*, 18420–18428.

(24) Wang, Q.; Xu, H.; Huang, W.; Pan, Z.; Zhou, H. Metal organic frameworks-assisted fabrication of CuO/Cu$_2$O for enhanced selective catalytic reduction of NO$_x$ by NH$_3$ at low temperatures. *J. Hazard. Mater.* **2019**, *364*, 499–508.

(25) Liu, W.; Lu, C.; Wang, X.; Liang, K.; Tay, B. K. In situ fabrication of three-dimensional, ultrathin graphite/carbon nanotube/NiO composite as binder-free electrode for high-performance energy storage. *J. Mater. Chem. A* **2015**, *3*, 624–633.

(26) Liu, X.; Liu, W.; Ko, M.; Park, M.; Kim, M. G.; Oh, P.; Chae, S.; Park, S.; Casimir, A.; Wu, G.; Cho, J. Metal (Ni, Co)-Metal Oxides/Graphene Nanocomposites as Multifunctional Electrocatalysts. *Adv. Funct. Mater.* **2015**, *25*, 5799–5808.

(27) Naveen, A. N.; Selladurai, S. Investigation on physiochemical properties of Mn substituted spinel cobalt oxide for supercapacitor applications. *Electrochim. Acta* **2014**, *125*, 404–414.

(28) Xia, W.; Zou, R.; An, L.; Xia, D.; Guo, S. A metal−organic framework route to in situ encapsulation of Co@Co$_3$O$_4$@C core@bishell nanoparticles into a highly ordered porous carbon matrix for oxygen reduction. *Energy Environ. Sci.* **2015**, *8*, 568–576.

(29) Yu, K.; Lou, L. L.; Liu, S.; Zhou, W. Asymmetric Oxygen Vacancies: the Intrinsic Redox Active Sites in Metal Oxide Catalysts. *Adv. Sci.* **2020**, *7*, No. 1901970.

(30) Zhang, S.-Y.; Li, T.-T.; Zhu, H.-L.; Zheng, Y.-Q. Co$_3$O$_4$ polyhedrons with enhanced electric conductivity as efficient water oxidation electrocatalysts in alkaline medium. *J. Mater. Sci.* **2018**, *53*, 4323–4333.

(31) Arend, M.; Nonnen, T.; Hoelderich, W. F.; Fischer, J.; Groos, J. Catalytic deoxygenation of oleic acid in continuous gas flow for the production of diesel-like hydrocarbons. *Appl. Catal., A* **2011**, *399*, 198–204.

(32) Cipriani, G.; Di Dio, V.; Genduso, F.; La Cascia, D.; Liga, R.; Miceli, R.; Galluzzo, G. R. Perspective on hydrogen energy carrier and its automotive applications. *Int. J. Hydrogen Energy* **2014**, *39*, 8482–8494.

(33) Wu, J. H.; Wang, T. F.; Fu, J.; Hou, Z. Y.; Lu, X. Y. Mechanism for the Controllable Production of Heptadecane by Hydrothermal In-Situ Hydrogenation and Decarboxylation of Oleic Acid with Methanol. *Energy Environ. Focus* **2016**, *5*, 163–168.

(34) Cao, Y.; Shi, Y.; Bi, Y.; Wu, K.; Hu, S.; Wu, Y.; Huang, S. Hydrodeoxygenation and hydroisomerization of palmitic acid over bi-functional Co/H-ZSM-22 catalysts. *Fuel Process. Technol.* **2018**, *172*, 29–35.

(35) Kwon, K. C.; Mayfield, H.; Marolla, T.; Nichols, B.; Mashburn, M. Catalytic deoxygenation of liquid biomass for hydrocarbon fuels. *Renewable Energy* **2011**, *36*, 907–915.

(36) Asikin-Mijan, N.; Lee, H. V.; Abdulkareem-Alsultan, G.; Afandi, A.; Taufiq-Yap, Y. H. Production of green diesel via cleaner catalytic deoxygenation of Jatropha curcas oil. *J. Cleaner Prod.* **2017**, *167*, 1048–1059.

(37) Li, M.; Fu, J.; Xing, S.; Yang, L.; Zhang, X.; Lv, P.; Wang, Z.; Yuan, Z. A novel catalyst with variable active sites for the direct hydrogenation of waste oils into jet fuel. *Appl. Catal., B* **2020**, *260*, No. 118114.

(38) Reangchim, P.; Saelee, T.; Itthibenchapong, V.; Junkaew, A.; Chanlek, N.; Eiad-ua, A.; Kungwan, N.; Faungnawakij, K. Role of Sn promoter in Ni/Al$_2$O$_3$ catalyst for the deoxygenation of stearic acid and coke formation: experimental and theoretical studies. *Catal. Sci. Technol.* **2019**, *9*, 3361–3372.

(39) Kaewmeesri, R.; Srifa, A.; Itthibenchapong, V.; Faungnawakij, K. Deoxygenation of Waste Chicken Fats to Green Diesel over Ni/Al$_2$O$_3$: Effect of Water and Free Fatty Acid Content. *Energy Fuels* **2015**, *29*, 833–840.

(40) Lestari, S.; Mäki-Arvela, P.; Simakova, I.; Beltramini, J.; Lu, G. Q. M.; Murzin, D. Y. Catalytic Deoxygenation of Stearic Acid and Palmitic Acid in Semibatch Mode. *Catal. Lett.* **2009**, *130*, 48–51.